ISSN 1392-1207. MECHANIKA. Vol. 32, No. 5, 2026: 348–358

Dynamic Stability of an S-FGMs Micro Shell with Temperature–Dependent Properties Subjected to a Swirling Annular Flow Considering Fluid Viscosity

Wen-Bo NING, Xinping XU, Yue ZHOU
Jiangsu Key Laboratory of Advanced Manufacturing Technology, Huai'an University, Huai'an 223003, China,
E-mail: wbnhyit@hau.edu.cn (Corresponding Author: Wen-Bo NING)
https://doi.org/10.5755/j02.mech.44274

1. Introduction

Shell-type structural elements have been widely used in aerospace engineering and biomechanical applications. With the development of micro/nano - electro - mechanical system (M/NEMS) [1], micro-shell-like structures are frequently encountered. The responses of such micro structures subjected to various loadings are described using non-classical theories accounting for the size effect. The modified couple stress theory [2], which is becoming popular in the analysis of microscale structures because of the involvement of only one material length scale parameter, has been successfully applied to investigate the dynamic behaviors of micro/nano plates and shells. The modified couple stress theory has been successfully applied to study buckling and the dynamic behaviors of micro/nano beams and plates [3, 4]. Sahmani et al. [5] presented the dynamic response of cylindrical microshells based on the modified couple stress theory. These studies have proved that the modified couple stress theory is effective and feasible.

Because the material properties vary smoothly and continuously through the thickness direction, functionally graded materials (FGMs) possess the advantages of high-temperature resistance and low stress concentration, and FGMs have been developed for use as macro/micro-scale elements in high temperature environment. To reduce the stress intensity factors, the new sigmoid FGMs (S-FGMs) were proposed by Chung and Chi [6].

Fluid-conveying micro/nano-pipes/tubes/shells have important applications in micro/nano devices, such as micro/nano-pumps, micro/nano-biosensors, micro/nano-mixtures, etc. [7, 8]. Dynamic responses of fluid-conveying micro/nano-pipes and shells have been studied extensively. These early studies focused on determining the natural frequency and the fluid velocity at which instability occurs (i.e., critical flow velocity) based on linear theory. Zhou and Wang [9] studied the vibrations and stability of a micro-pipe carrying fluid, and they found the fluid velocity has a pronounced effect on the vibration analysis. Recently, the nonlinear theory for the vibration and stability of fluid-conveying micro/nano-structures has been reported. Mashrouteh [10] investigated the nonlinear free vibration of fluid-conveying microtubes based on the modified couple stress theory. They obtained analytical expressions for nonlinear natural frequencies and the time responses of different vibration modes using the variational iteration method. Based on the modified couple stress theory, the effects of loose supports and visco-Pasternak medium are further taken into account to study the nonlinear behaviors of fluid-conveying micropipes [11]. These studies have shown that the material length-scale parameter plays an important role in the instability analysis of fluid-conveying micro-pipes, tubes and shells.

The fluid viscosity was also considered by diverse fluid modeling strategies [12, 13]. In general, the fluid viscosity has a destabilizing effect on fluid-conveying micro-pipes, tubes and shells.

Micro- or nano-pipes/tubes/shells are often found in thermal environments. The temperature change may induce the instability and vibrations of such structures. Some work on thermally induced vibrations, instability and bending of functionally graded material porous microtubes based on the modified couple stress theory was performed by Babaei and Eslami [14]. It was found that the critical instability temperature rise of FGMs micro tubes is higher when the FGMs properties are assumed to be temperature-dependent. Wang et al. [15] reported the thermal effects on the vibration and instability of fluid-conveying carbon nanotubes based on the Bernoulli–Euler beam model. They found that the temperature variations could influence the natural frequency and critical flow velocity. The same problem was further studied by Askari and Esmailzadeh [16]. They revealed the effects of different parameters, such as temperature change, nonlinear foundation, and surface stress, on linear and nonlinear vibrations of fluid-conveying carbon nanotubes. Furthermore, the effects of the structural damping and external fluid viscosity were elucidated [17]. Tong et al. [18] presented the thermal-elastic vibration analyses of functionally graded micropipes carrying fluid. For different non-classical theories, they all agreed that the natural frequency and critical velocity of the system would decrease with increasing temperature rise. The further research in this area was extended to study stability behavior of an FGMs micro-shell subjected to swirling annular flow [19]. Annular flow in micro channels is of great importance in microfluidic devices and chemical and heat transfer applications. Micro-reactors and annular micro-mixers are good examples [20]. It was found that the Reynolds number for transition to turbulence is lower than that observed at macro-scale [21]. Thus, fluid flow in micro- channels is assumed to be turbulent in the present work.

From the above literature, there are few studies on stability analysis of FGMs micro-shells subjected to swirling annular flow in thermal environments. The present FGMs micro-shell with metal-ceramic-metal layers is called an S-FGM shell. Based on the modified couple stress theory and Hamilton's principle, the governing equations of motion are derived including the fluid viscosity effect. By employing the zero-level contour method, the motion equations are solved with the aid of the programmed software

MATLAB. The complex dynamics of S-FGM micro-shells conveying swirling annular flow under thermal loads are investigated. The results of this study will be helpful in the optimum design of micro-scale shell structures.

2. Theoretical Model

2. 1. The statement of problem

Consider two coaxial S-FGMs micro-shells with the same length L subjected to swirling annular flow, as shown in Fig. 1. Here, the inner micro-shell is of mean radius r_i, and wall thickness h_i; the outer micro-shell is mean radius r_o, thickness h_o. The fluid-micro-shell system is defined in a cylindrical coordinate system (O; r, θ, x), where O is the origin point; x, θ, and r are in the axial, circumferential, and radial directions, respectively. The viscous flowing fluid through an annular gap between the two micro-shells is denoted by U_o and V_o along x- and θ- directions in time-average sense, and its density is ρ_f. Suppose that the two micro-shells exposed to the thermal field are dependent on temperature rise.

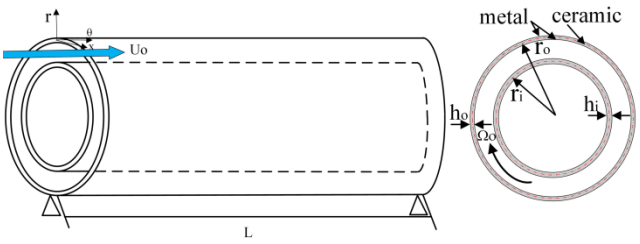

Fig. 1 Geometry and coordinate of coaxial S-FGMs micro-shells subjected to swirling annular flow

It is assumed that the fluid in the annular space is incompressible, fully developed turbulent flow, as reported in the literature [19]. The iterative solution of the Navier-Stokes equations by numerical means would entail high computational costs. Therefore, the fluid field may be decoupled, and the fluid forces acting on the shell wall may be divided into two sets of loads: the steady viscous forces, which can be determined separately in a time-averaged sense based on the time-mean Navier-Stokes equations; the inviscid fluid forces, which are obtained in a perturbation sense based on the potential flow theory [19].

We put forward these assumptions in the present paper.

1. Shell motions are so small that linear analysis is applicable;
2. Shell material properties are dependent on temperature;
3. The couple stress theory for fluid is not considered.

2. 2. Hydrodynamic pressure

Under the above assumptions, the present fluid is inviscid, irrotational, and incompressible. The hydrodynamic pressure exerted on the inner and outer shell walls can be expressed as [19]

$$p_i=-\frac{\rho_f}{\Gamma}\left(\frac{\partial}{\partial t}+\frac{V_o}{r}\frac{\partial}{\partial\theta}+U_o\frac{\partial}{\partial x}\right)^2\times \times\begin{Bmatrix}\left[I_n(\lambda r_i)K_n'(\lambda r_o)-I_n'(\lambda r_o)K_n(\lambda r_i)\right]w_i+\\+\left[I_n'(\lambda r_i)K_n(\lambda r_i)-I_n(\lambda r_i)K_n'(\lambda r_i)\right]w_o\end{Bmatrix}, \tag{1a}$$

$$p_o=-\frac{\rho_f}{\Gamma}\left(\frac{\partial}{\partial t}+\frac{V_o}{r}\frac{\partial}{\partial\theta}+U_o\frac{\partial}{\partial x}\right)^2\times \times\begin{Bmatrix}\left[I_n(\lambda r_o)K_n'(\lambda r_o)-I_n'(\lambda r_o)K_n(\lambda r_o)\right]w_i+\\+\left[I_n'(\lambda r_i)K_n(\lambda r_o)-I_n(\lambda r_o)K_n'(\lambda r_i)\right]w_o\end{Bmatrix}, \tag{1b}$$

in which $\Gamma=I_n'(\lambda r_i)K_n'(\lambda r_o)-I_n'(\lambda r_o)K_n'(\lambda r_i)$; the tangential mean velocity $V_o=\Omega_o\times r$; the subscripts i, o pertain to the inner shell and outer shell; t denotes time; I_n, K_n are the modified Bessel functions of the first and second kind of order n; the prime denotes the differentiation with respect to the argument of the primed function; λ is the order of the axial vibration model; $w_{i/o}$ represents r-direction displacement of a shell.

When either of the two coaxial shells is perfectly stiff, the simplified form of the Eq. (1) can be obtained. Thus,

$$p_i=-\frac{\rho_f}{\Gamma}\left(\frac{\partial}{\partial t}+\frac{V_o}{r}\frac{\partial}{\partial\theta}+U_o\frac{\partial}{\partial x}\right)^2\times \times\left[I_n(\lambda r_i)K_n'(\lambda r_o)-I_n'(\lambda r_o)K_n(\lambda r_i)\right]w_i, \tag{2a}$$

$$p_o=-\frac{\rho_f}{\Gamma}\left(\frac{\partial}{\partial t}+\frac{V_o}{r}\frac{\partial}{\partial\theta}+U_o\frac{\partial}{\partial x}\right)^2\times \times\left[I_n'(\lambda r_i)K_n(\lambda r_o)-I_n(\lambda r_o)K_n'(\lambda r_i)\right]w_o. \tag{2b}$$

2. 3. Derivation of the steady viscous forces

Considering fluid rotation of annular flow, the time-mean Navier-Stokes equations may be modified

$$\frac{1}{\rho_f}\frac{\partial P}{\partial x}=-\frac{1}{r}\frac{d}{dr}\left(r\overline{u_x u_r}\right)+\frac{\nu}{r}\frac{d}{dr}\left(r\frac{dU_o}{dr}\right), \tag{3a}$$

$$\frac{1}{\rho_f}\frac{\partial P}{\partial r}=-\frac{1}{r}\frac{d}{dr}\left(r\overline{u_r^2}\right)+\frac{1}{r}\left(\overline{u_\theta^2}\right)+\frac{V_o^2}{r}, \tag{3b}$$

$$0=\frac{d}{dr}\left(\overline{u_r u_\theta}\right)+\frac{2}{r}\left(\overline{u_r u_\theta}\right)+\nu\left(\frac{\partial^2 V_o}{\partial r^2}+\frac{1}{r}\frac{\partial V_o}{\partial r}-\frac{V_o}{r^2}\right). \tag{3c}$$

The continuity equation of annular flow is given

$$\frac{\partial U_o}{\partial x}+\frac{1}{r}\frac{\partial(rV_o)}{\partial r}=0, \tag{4}$$

where P denotes the static pressure; $\overline{(\,)}$ indicates the time mean of ( ); u_x, u_y and u_θ are fluctuating velocity components of turbulent flow along the x-, r-, and θ- directions, respectively; ν is the fluid kinematic viscosity.

Based on the assumption of fully developed turbulent flow and the boundary conditions of fluctuating velocities, the desired results are given below after the lengthy mathematical manipulation. The details of derivations have been given [19], and are not repeated here.

$$P_{ro}=-\left[\frac{2r_o}{r_o^2-r_m^2}\right]\rho_f U_{\tau o}{}^2 x+\rho_f\int_{r_i}^{r_o}\frac{1}{r}\left(\overline{u_\theta^2}-\overline{u_r^2}\right)dr+ +0.5\rho_f\Omega_o{}^2\left(r_o^2-r_i^2\right)+P(0,r_o)-p_e, \tag{5a}$$

$$P_{xo}=\rho_f U_{\tau o}^2, \tag{5b}$$

$$P_{\theta o}=\rho_f\nu\left[\frac{\mathrm{d}V_o}{\mathrm{d}r}-\frac{V_o}{r}\right]_{r=r_o}=-\rho_f\nu\frac{2H}{r^2}= =-2\rho_f\nu\Omega_o, \tag{5c}$$

where the fluid rotation speed $\Omega_o=\frac{V_o}{r}$;

$U_{\tau o}{}^2=\frac{1}{8}f\frac{r_o{}^2-r_m{}^2}{r_o(r_o-r_i)}U_o{}^2$. Here, the friction factor f is a complex function of the Reynolds number Re and of the relative roughness of a shell Δ/d, and the empirical expression is given by Haaland [22]

$$\frac{1}{f}=-1.8log_{10}\left[\left(\frac{\Delta}{3.7d}\right)^{1.11}+\frac{6.9}{Re}\right], \tag{6}$$

where Δ is the average height of shell wall protrusions and $d=2(r_o-r_i)$ is the hydraulic diameter of the annular flow gap. The r_m appearing in Eq. (3) is the radius at which the fluid velocity is maximum and the expression of r_m is found to be [23]

$$r_m=\sqrt{\frac{r_o{}^2-r_i{}^2}{2ln\left(r_o/r_i\right)}}. \tag{7}$$

By balancing forces on a shell element, the above-obtained viscosity-related forces can be transformed into the stress resultants when the shells are simply supported [19]

$$\begin{aligned}&N_{\theta i/o}=P_{ri/o}r_{i/o},\\&N_{xi/o}=-P_{xi/o}\left(x-0.5L\right)^2+0.25P_{xi/o}L^2,\\&N_{x\theta i/o}=-P_{\theta i/o}\left(x-0.5L\right)^2+0.25P_{\theta i/o}L^2,\end{aligned} \tag{8}$$

here, N_x, N_θ are the axial and hoop stress resultants, while $N_{x\theta}$ is the shear stress resultant.

After lengthy mathematical manipulations, the dimensional terms $Q_{1,\,2,\,3,\,4i/o}$ are given [19]

$$\begin{aligned}&Q_{1i/o}=N_{xi/o},\ Q_{2i/o}=p_{xi/o}r_{i/o},\\&Q_{3i/o}=N_{\theta i/o},\ Q_{4i/o}=N_{x\theta i/o}.\end{aligned} \tag{9}$$

2. 4. The governing equations of S-FGMs shell motion

Consider an S-FGMs micro-shell with stainless steel-ceramic-stainless steel layers. An effective material property P_{eff} of the micro-shell, like elastic modulus E_{eff}, thermal expansion coefficient α_{eff}, and density $\rho_{s\,eff}$, is expressed as

$$P_{eff}=P_cV_c+P_mV_m, \tag{10}$$

where the subscripts c and m indicate the ceramic and stainless steel, respectively; P denotes the material property of the S-FGMs shell; V is the volume fraction.

The material properties are temperature-dependent and can be estimated by Touloukian [24]

$$P_{c/m}=P_0\left(P_{-1}T^{-1}+1+P_1T^1+P_2T^2+P_3T^3\right), \tag{11}$$

where $P_i\,(i=-1,\,0,\,1,\,2,\,3)$ indicates the shell material property constants and $T=T_o+\Delta T$; T_o is the room temperature 300 K and ΔT is the temperature rise.

According to the sigmoid power law, the volume fraction is given by

$$V_{c/m}(z)=\begin{cases}\left(\frac{2z+h}{h}\right)^N, & -\frac{h}{2}\le z\le 0\\ \left(\frac{-2z+h}{h}\right)^N, & 0\le z\le\frac{h}{2}\end{cases},\quad V_c+V_m=1, \tag{12}$$

where h is the shell thickness and z is the shell displacement variable along r-direction; N represents the volume index.

From the above equations, we can obtain

$$E(z,T)=E_sV_s+E_cV_c=E_s+\left(E_c-E_s\right)\times \times\begin{cases}\left(\frac{2z+h}{h}\right)^N, & -\frac{h}{2}\le z\le 0\\ \left(\frac{-2z+h}{h}\right)^N, & 0\le z\le\frac{h}{2}\end{cases}; \tag{13a}$$

$$\rho(z,T)=\rho_sV_s+\rho_cV_c=\rho_s+\left(\rho_c-\rho_s\right)\times \times\begin{cases}\left(\frac{2z+h}{h}\right)^N, & -\frac{h}{2}\le z\le 0\\ \left(\frac{-2z+h}{h}\right)^N, & 0\le z\le\frac{h}{2}\end{cases}; \tag{13b}$$

$$\alpha(z,T)=\alpha_sV_s+\alpha_cV_c=\alpha_s+\left(\alpha_c-\alpha_s\right)\times \times\begin{cases}\left(\frac{2z+h}{h}\right)^N, & -\frac{h}{2}\le z\le 0\\ \left(\frac{-2z+h}{h}\right)^N, & 0\le z\le\frac{h}{2}\end{cases}. \tag{13c}$$

It is evident that at $z=\pm h/2$, the S-FGMs shell is an isotropic stainless steel one. Whereas $z=0$, the S-FGMs shell is an isotropic ceramic one. Here the Poisson's ratio υ is constant.

Based on the modified couple stress theory [2], the strain energy in the volume Ω is defined by

$$U_e = \frac{1}{2}\int_{\Omega}\left(\sigma_{ij}:\varepsilon_{ij} + m_{ij}:\chi_{ij}\right)dq\,, \tag{14}$$

where σ_{ij}, ε_{ij}, m_{ij}, and χ_{ij} are respectively the stress tensor, Cauchy strain tensor, higher order stress tensor, and symmetric rotation gradient tensor; $i, j = x, \theta, r$.

These tensors can be expressed from the Love's shell theory [25]

$$\varepsilon_x = \frac{\partial u}{\partial x} - z\frac{\partial^2 w}{\partial x^2}\,, \tag{15a}$$

$$\varepsilon_\theta = \frac{\partial v}{r\partial\theta} + \frac{w}{r} - z\frac{\partial^2 w}{r^2\partial\theta^2} + z\frac{\partial v}{r^2\partial\theta}\,, \tag{15b}$$

$$\varepsilon_{x\theta} = \frac{\partial u}{r\partial\theta} + \frac{\partial v}{\partial x} - 2z\frac{\partial^2 w}{r\partial x\partial\theta} + 2z\frac{\partial v}{r\partial x}\,, \tag{15c}$$

where u, v and w are the x-, θ-, and r- directions displacements of a shell, respectively; z indicates a displacement variable of r- direction.

We assume that the temperature distribution is uniform and steady. According to Eslami's thermo-elastic theory [26], the only axial thermal load is non-zero while all other thermal loads are zero for a simply supported shell. Considering the thermal loads, the stress tensors can be obtained from Hooke's law

$$\begin{aligned}
\sigma_x &= \frac{E(z,T)}{1-\upsilon^2}\left[\varepsilon_x + \upsilon\varepsilon_\theta - (1+\upsilon)\alpha(z,T)\Delta T\right],\\
\sigma_\theta &= \frac{E(z,T)}{1-\upsilon^2}\left(\varepsilon_\theta + \upsilon\varepsilon_x\right),\\
\tau_{x\theta} &= \frac{E(z,T)}{2(1+\upsilon)}\varepsilon_{x\theta}.
\end{aligned} \tag{16}$$

The force and moment resultants of a shell are obtained by integrating along the shell thickness.

$$N_x = \int_{-h/2}^{h/2}\sigma_x dz = \frac{E_1 h}{1-\upsilon^2}\left(\frac{\partial u}{\partial x} + \upsilon\frac{\partial v}{r\partial\theta} + \upsilon\frac{w}{r}\right) - \frac{E_2 h^2}{1-\upsilon^2}\left(\frac{\partial^2 w}{\partial x^2} + \upsilon\frac{\partial^2 w}{r^2\partial\theta^2} - \upsilon\frac{\partial v}{r^2\partial\theta}\right) - N_x^{\,T}, \tag{17a}$$

$$N_\theta = \int_{-h/2}^{h/2}\sigma_\theta dz = \frac{E_1 h}{1-\upsilon^2}\left(\upsilon\frac{\partial u}{\partial x} + \frac{\partial v}{r\partial\theta} + \frac{w}{r}\right) - \frac{E_2 h^2}{1-\upsilon^2}\left(\upsilon\frac{\partial^2 w}{\partial x^2} + \frac{\partial^2 w}{r^2\partial\theta^2} - \frac{\partial v}{r^2\partial\theta}\right), \tag{17b}$$

$$N_{x\theta} = \int_{-h/2}^{h/2}\tau_{x\theta} dz = \frac{E_1 h}{2(1+\upsilon)}\left(\frac{\partial u}{r\partial\theta} + \frac{\partial v}{\partial x}\right) - \frac{E_2 h^2}{(1+\upsilon)}\left(\frac{\partial^2 w}{r\partial x\partial\theta} - \frac{\partial v}{r\partial x}\right), \tag{17c}$$

$$M_x = \int_{-h/2}^{h/2}\sigma_x z dz = \frac{E_2 h^2}{1-\upsilon^2}\frac{\partial u}{\partial x} + \frac{\upsilon E_2 h^2}{1-\upsilon^2}\left(\frac{\partial v}{r\partial\theta} + \frac{w}{r}\right) - \frac{E_3 h^3}{(1-\upsilon^2)}\left(\frac{\partial^2 w}{\partial x^2} + \upsilon\frac{\partial^2 w}{r^2\partial\theta^2} - \upsilon\frac{\partial v}{r^2\partial\theta}\right), \tag{17d}$$

$$M_\theta = \int_{-h/2}^{h/2}\sigma_\theta z dz = \frac{\upsilon E_2 h^2}{1-\upsilon^2}\frac{\partial u}{\partial x} + \frac{E_2 h^2}{1-\upsilon^2}\left(\frac{\partial v}{r\partial\theta} + \frac{w}{r}\right) - \frac{E_3 h^3}{(1-\upsilon^2)}\left(\upsilon\frac{\partial^2 w}{\partial x^2} + \frac{\partial^2 w}{r^2\partial\theta^2} - \frac{\partial v}{r^2\partial\theta}\right), \tag{17e}$$

$$M_{x\theta} = \int_{-h/2}^{h/2}\tau_{x\theta} z dz = \frac{E_2 h^2}{2(1+\upsilon)}\left(\frac{\partial u}{r\partial\theta} + \frac{\partial v}{\partial x}\right) - \frac{E_3 h^3}{(1+\upsilon)}\left(\frac{\partial^2 w}{r\partial x\partial\theta} - \frac{\partial v}{r\partial x}\right), \tag{17f}$$

$$N_x^{\,T} = \frac{E_1\alpha_1}{1-\upsilon^2}(1+\upsilon)\Delta T, \tag{17g}$$

where

$$\begin{aligned}
E_1 &= \int_{-h/2}^{h/2}E(z,T)dz = E_s h + \frac{(E_c - E_s)h}{N+1}\,,\\
E_2 &= \int_{-h/2}^{h/2}E(z,T)z dz = 0\,,\\
E_3 &= \int_{-h/2}^{h/2}E(z,T)z^2 dz = \frac{E_s h^3}{12} + \frac{(E_c - E_s)h^3}{2(N+1)(N+2)(N+3)},\\
\alpha_1 &= \int_{-h/2}^{h/2}\alpha(z,T)dz = \alpha_s h + \frac{(\alpha_c - \alpha_s)h}{N+1}\,.
\end{aligned}$$

According to Kirchhoff's hypotheses, the symmetric rotation gradient tensors can be expressed as

$$\begin{aligned}
&\chi_x = \frac{1}{2}\frac{\partial^2 w}{r\partial x\partial\theta},\ \chi_\theta = -\frac{1}{2}\frac{\partial^2 w}{r\partial x\partial\theta},\\
&\chi_{x\theta} = \frac{1}{4}\left(\frac{\partial^2 w}{r^2\partial\theta^2} - \frac{\partial^2 w}{\partial x^2}\right),\ \chi_z = 0,
\end{aligned} \tag{18a}$$

$$\begin{aligned}
\chi_{xz} &= \frac{1}{4}\left(\frac{\partial^2 v}{\partial x^2} - \frac{\partial^2 u}{r\partial x\partial\theta}\right),\\
\chi_{\theta z} &= \frac{1}{4}\left(\frac{\partial^2 v}{r\partial x\partial\theta} - \frac{\partial^2 u}{r^2\partial\theta^2}\right),
\end{aligned} \tag{18b}$$

$$\gamma_{ij} = 2l^2 G\chi_{ij}\,. \tag{19}$$

Here, l is the material length-scale parameter; G is the shear modulus.

According to the relationship between the higher-order stress tensor and the symmetric rotation gradient tensor, the couple forces γ_{ij} and the couple moments t_{ij} are given by

$$\gamma_x=\frac{E_1l^2h}{(1+\upsilon)}\chi_x,\ \gamma_\theta=\frac{E_1l^2h}{(1+\upsilon)}\chi_\theta,$$
$$\gamma_{x\theta}=\frac{E_1l^2h}{(1+\upsilon)}\chi_{x\theta},\ \gamma_{xz}=\frac{E_1l^2h}{(1+\upsilon)}\chi_{xz},\tag{20a}$$
$$\gamma_{\theta z}=\frac{E_1l^2h}{(1+\upsilon)}\chi_{\theta z},$$

$$t_x=\frac{E_2l^2h^2}{(1+\upsilon)}\chi_x,\ t_\theta=\frac{E_2l^2h^2}{(1+\upsilon)}\chi_\theta,$$
$$t_{x\theta}=\frac{E_2l^2h^2}{(1+\upsilon)}\chi_{x\theta},\ t_{xz}=\frac{E_2l^2h^2}{(1+\upsilon)}\chi_{xz},\tag{20b}$$
$$t_{\theta z}=\frac{E_2l^2h^2}{(1+\upsilon)}\chi_{\theta z}.$$

According to Hamilton's variational principle, the motion equations of a shell conveying fluid are produced by

$$\frac{\partial N_x}{\partial x}+\frac{1}{r}\frac{\partial N_{x\theta}}{\partial\theta}+(Q_1-N_x{}^T)\frac{\partial^2u}{\partial x^2}+Q_2\left(\frac{\partial v}{r^2\partial\theta}+\frac{w}{r^2}\right)+$$
$$+Q_3\left(\frac{\partial^2u}{r^2\partial\theta^2}-\frac{\partial w}{r\partial x}\right)+2Q_4\frac{\partial^2u}{r\partial x\partial\theta}+\frac{1}{2}\frac{\partial^2\gamma_{xz}}{r\partial x\partial\theta}+$$
$$+\frac{1}{2}\frac{\partial^2\gamma_{\theta z}}{r^2\partial\theta^2}+\frac{1}{2}\frac{\partial^2t_{xz}}{r\partial x\partial\theta}+\frac{1}{2}\frac{\partial^2t_{\theta z}}{r^2\partial\theta^2}=\rho_s\frac{\partial^2u}{\partial t^2},\tag{21a}$$

$$\frac{\partial N_{x\theta}}{\partial x}+\frac{1}{r}\frac{\partial N_\theta}{\partial\theta}+\left(Q_1-N_x{}^T\right)\frac{\partial^2v}{\partial x^2}+$$
$$+Q_3\left(\frac{\partial^2v}{r^2\partial\theta^2}+\frac{\partial w}{r^2\partial\theta}\right)+2Q_4\left(\frac{\partial^2v}{r\partial x\partial\theta}+\frac{\partial w}{r\partial x}\right)-$$
$$-\frac{1}{2}\frac{\partial^2\gamma_{xz}}{\partial x^2}-\frac{1}{2}\frac{\partial^2\gamma_{\theta z}}{r\partial x\partial\theta}-$$
$$-\frac{1}{2}\frac{\partial^2t_{xz}}{\partial x^2}-\frac{1}{2}\frac{\partial^2t_{\theta z}}{r\partial x\partial\theta}=\rho_s\frac{\partial^2v}{\partial t^2},\tag{21b}$$

$$\frac{\partial^2M_x}{\partial x^2}+\frac{2}{r}\frac{\partial^2M_{x\theta}}{\partial x\partial\theta}+\frac{1}{r^2}\frac{\partial^2M_\theta}{\partial\theta^2}-\frac{N_\theta}{r}+$$
$$+\left(Q_1-N_x{}^T\right)\frac{\partial^2w}{\partial x^2}+Q_3\left(\frac{\partial u}{r\partial x}-\frac{\partial v}{r^2\partial\theta}+\frac{\partial^2w}{r^2\partial\theta^2}\right)+$$
$$+2Q_4\left(\frac{\partial v}{r\partial x}-\frac{\partial^2w}{r\partial x\partial\theta}\right)-\frac{1}{r}\frac{\partial^2\gamma_x}{\partial x\partial\theta}+\frac{1}{r}\frac{\partial\gamma_\theta}{\partial x\partial\theta}-$$
$$-\frac{1}{2}\frac{\partial^2\gamma_{x\theta}}{r^2\partial\theta^2}+\frac{1}{2}\frac{\partial^2\gamma_{x\theta}}{\partial x^2}-\frac{1}{r}\frac{\partial^2t_x}{\partial x\partial\theta}+$$
$$+\frac{1}{r}\frac{\partial t_\theta}{\partial x\partial\theta}-\frac{1}{2}\frac{\partial^2t_{x\theta}}{r^2\partial\theta^2}+\frac{1}{2}\frac{\partial^2t_{x\theta}}{\partial x^2}=\rho_s\frac{\partial^2w}{\partial t^2}+p_{i/o},\tag{21c}$$

where $\rho_s=\int_{-h/2}^{h/2}\rho(z,T)dz=\rho_sh+\frac{\rho_c-\rho_s}{N+1}h$.

Introducing the expressions of forces, moments and couple stresses into Eqs. (21), the motion equations of the shell can be rewritten in the form of a linear matrix operator

$$\zeta\begin{bmatrix}u_{i/o}\\v_{i/o}\\w_{i/o}\end{bmatrix}=\begin{bmatrix}0\\0\\p_{i/o}\end{bmatrix},\tag{22}$$

where:

$$\zeta=\frac{E_1}{1-\upsilon^2}\begin{bmatrix}\zeta_{11}&\zeta_{12}&\zeta_{13}\\\zeta_{21}&\zeta_{22}&\zeta_{23}\\\zeta_{31}&\zeta_{32}&\zeta_{33}\end{bmatrix},$$

$$\zeta_{11}=\left(1+Q_1'-(1+\upsilon)\alpha_1\Delta T\right)\frac{\partial^2}{\partial x^2}+\left(\frac{1-\upsilon}{2}+Q_3'\right)\frac{\partial^2}{r^2\partial\theta^2}+$$
$$+2Q_4'\frac{\partial^2}{r\partial x\partial\theta}-l^2\frac{1-\upsilon}{2r^2}\frac{\partial^4}{\partial x^2\partial\theta^2}-l^2\frac{1-\upsilon}{2r^4}\frac{\partial^4}{\partial\theta^4}-$$
$$-l^2\frac{E_2}{E_1}\frac{1-\upsilon}{2r^2}\frac{\partial^4}{\partial x^2\partial\theta^2}-l^2\frac{E_2}{E_1}\frac{1-\upsilon}{2r^4}\frac{\partial^4}{\partial\theta^4}-\rho_s\frac{1-\upsilon^2}{E_1}\frac{\partial^2}{\partial t^2},$$

$$\zeta_{12}=\zeta_{21}=\frac{1+\upsilon}{2r}\frac{\partial^2}{\partial x\partial\theta}+Q_2'\frac{\partial}{r^2\partial\theta}+l^2\frac{1-\upsilon}{2r}\frac{\partial^4}{\partial x^3\partial\theta}+$$
$$+l^2\frac{1-\upsilon}{2r^3}\frac{\partial^4}{\partial x\partial\theta^3}+l^2\frac{E_2}{E_1}\frac{1-\upsilon}{2r}\frac{\partial^4}{\partial x^3\partial\theta}+l^2\frac{E_2}{E_1}\frac{1-\upsilon}{2r^3}\frac{\partial^4}{\partial x\partial\theta^3},$$

$$\zeta_{13}=\zeta_{31}=\left(\upsilon_1-Q_3'\right)\frac{\partial}{r\partial x}+Q_2'\frac{1}{r^2}-\frac{E_2}{E_1}\frac{\partial^3}{\partial x^3}-$$
$$-\frac{E_2}{r^2E_1}\frac{\partial^3}{\partial x\partial\theta^2},$$

$$\zeta_{22}=\left(\frac{1-\upsilon}{2}+Q_1'-(1+\upsilon)\alpha_1\Delta T\right)\frac{\partial^2}{\partial x^2}+2Q_4'\frac{\partial^2}{r\partial x\partial\theta}+$$
$$+\left(1+Q_3'\right)\frac{\partial^2}{r^2\partial\theta^2}-l^2\frac{1-\upsilon}{2}\frac{\partial^4}{\partial x^4}-l^2\frac{1-\upsilon}{2r^2}\frac{\partial^4}{\partial x^2\partial\theta^2}-$$
$$-l^2\frac{E_2}{E_1}\frac{1-\upsilon}{2}\frac{\partial^4}{\partial x^4}-l^2\frac{E_2}{E_1}\frac{1-\upsilon}{2r^2}\frac{\partial^4}{\partial x^2\partial\theta^2}-\rho_s\frac{1-\upsilon^2}{E_1}\frac{\partial^2}{\partial t^2},$$

$$\zeta_{23}=\zeta_{32}=\left(\upsilon+Q_3'\right)\frac{1}{r^2}\frac{\partial}{\partial\theta}+2Q_4'\frac{\partial}{r\partial x}-$$
$$-\frac{E_2}{rE_1}\frac{1-\upsilon}{2}\frac{\partial^3}{\partial x^2\partial\theta}-\frac{E_2}{r^3E_1}\frac{1-\upsilon}{2}\frac{\partial^3}{\partial\theta^3},$$

$$\zeta_{33}=\left(-Q_1'+(1+\upsilon)\alpha_1\Delta T\right)\frac{\partial^2}{\partial x^2}-2Q_4'\frac{\partial^2}{r\partial x\partial\theta}+$$
$$+Q_3'\frac{\partial^2}{r^2\partial\theta^2}+\frac{1}{r^2}+\frac{h^2}{12r^4}+\frac{h^2}{12}+\frac{E_3}{E_1}\Delta\Delta-\frac{2\upsilon_2E_2}{rE_1}\frac{\partial^2}{\partial x^2}-$$
$$-\frac{2E_2}{r^3E_1}\frac{\partial^2}{\partial\theta^2}+\rho_s\frac{1-\upsilon^2}{E_1}\frac{\partial^2}{\partial t^2}+l^2\frac{1-\upsilon}{2}\frac{\partial^4}{\partial x^4}+l^2\frac{1-\upsilon}{2r^4}\frac{\partial^4}{\partial\theta^4}+$$
$$+l^2\frac{1-\upsilon}{2r^2}\frac{\partial^4}{\partial x^2\partial\theta^2}l^2+\frac{E_2}{E_1}\frac{1-\upsilon}{2}\frac{\partial^4}{\partial x^4}+l^2\frac{E_2}{E_1}\frac{1-\upsilon}{2r^4}\frac{\partial^4}{\partial\theta^4}+$$
$$+l^2\frac{E_2}{E_1}\frac{1-\upsilon}{2r^2}\frac{\partial^4}{\partial x^2\partial\theta^2}.$$

In which,

$$\Delta=\frac{\partial^2}{\partial x^2}+\frac{1}{r^2}\frac{\partial^2}{\partial\theta^2};\ Q_1'=\frac{1-\upsilon^2}{E_1}N_x;\ Q_2'=\frac{r1\left(-\upsilon^2\right)}{E_1}p_x;$$

$$Q_3'=\frac{1-\upsilon^2}{E_1}N_\theta;\ Q_4'=\frac{1-\upsilon^2}{E_1}N_{x\theta}.$$

2.5. Method of solution

It has been proved that the travelling-wave type solution used for stability analysis of fluid-filled shells is valid [27]. By expanding the displacement components in the form of travelling-wave, the displacements *u, v* and *w* of the inner or outer shell with simply supported boundary conditions can be expressed as [27]

$$\begin{bmatrix} u_{i/o} \\ v_{i/o} \\ w_{i/o} \end{bmatrix} = \begin{bmatrix} u_{mn}\, exp\left[-i\left(\lambda x + n\theta - \omega t\right)\right] \\ v_{mn}\, exp\left[-i\left(\lambda x + n\theta - \omega t\right)\right] \\ w_{mn}\, exp\left[-i\left(\lambda x + n\theta - \omega t + \pi/2\right)\right] \end{bmatrix},$$

$$\left(\lambda = \frac{m\pi}{L}\right), \tag{23}$$

were m is axial half wavenumber, n is circumferential wavenumber; ω indicates the circular frequency.

The motion equations can be nondimensionalized by introducing the reference time τ

$$\tau = r_i\sqrt{\frac{\rho_s\left(1-\upsilon^2\right)}{E}}$$

and leading to

$$\bar{l} = \frac{l}{r_i},\ \bar{t} = \frac{t}{\tau},\ \bar{h} = \frac{h}{r_i},\ \bar{x} = \frac{x}{r_i},\ \bar{L} = \frac{L}{r_i},\ \bar{r} = \frac{r}{r_i},$$

$$\bar{p} = \frac{\tau^2}{\rho_s r_i^2}p,\ \overline{U_o} = \frac{U_o\tau}{r_i},\ \overline{\Delta T} = \frac{\Delta T}{T_o},$$

$$\overline{V_o} = \frac{V_o\tau}{r_i},\ \lambda_c = \frac{r_o}{r_i},\ k = \frac{r_o - r_i}{r_i},\ \bar{\omega} = \omega\tau,$$

$$\overline{Q_{1,2,3,4}} = \frac{\tau^2}{\rho_s r_i^2}Q_{1,2,3,4},$$

$$\begin{bmatrix} \overline{u_{i/o}} \\ \overline{v_{i/o}} \\ \overline{w_{i/o}} \end{bmatrix} = \frac{1}{r_i}\begin{bmatrix} u_{i/o} \\ v_{i/o} \\ w_{i/o} \end{bmatrix}. \tag{24}$$

In the case of the elastic outer shell and perfectly rigid inner shell in this paper, allowing for Eq. (2b), Eq. (11), and Eq. (24), the dimensionless form of Eq. (22) is obtained

$$\boldsymbol{\zeta u} = \boldsymbol{\zeta}\begin{bmatrix} \overline{u_o} \\ \overline{v_o} \\ -i\overline{w_o} \end{bmatrix} = \begin{bmatrix} 0 \\ 0 \\ 0 \end{bmatrix}, \tag{25}$$

where:

$$\boldsymbol{\zeta} = \begin{bmatrix} \zeta_{11} & \zeta_{12} & \zeta_{13} \\ \zeta_{21} & \zeta_{22} & \zeta_{23} \\ \zeta_{31} & \zeta_{32} & \zeta_{33} \end{bmatrix},$$

$$\zeta_{11} = \left(1 + \overline{Q_1} - (1+\upsilon)\alpha_1\overline{\Delta T}\right)\left(-\lambda^2\right) + \left(\frac{1-\upsilon}{2} + \overline{Q_3}\right)\frac{-n^2}{\lambda_c^2} +$$
$$+2\overline{Q_4}\frac{-\lambda n}{\lambda_c} - \bar{l}^2\frac{(1-\upsilon)\lambda^2 n^2}{2\lambda_c^2} - \bar{l}^2\frac{(1-\upsilon)n^4}{2\lambda_c^4} -$$
$$-\bar{l}^2\frac{\overline{E_2}}{\overline{E_1}}\frac{(1-\upsilon)\lambda^2 n^2}{2\lambda_c^2} - \bar{l}^2\frac{\overline{E_2}}{\overline{E_1}}\frac{(1-\upsilon)n^4}{2\lambda_c^4} - \rho_s\frac{1-\upsilon^2}{\overline{E_1}}\bar{\omega}^2,$$

$$\zeta_{12} = \zeta_{21} = -\frac{1+\upsilon}{2\lambda_c}\lambda n - \overline{Q_2}\frac{in}{\lambda_c^2} + \bar{l}^2\frac{(1-\upsilon)\lambda^3 n}{2\lambda_c} +$$
$$+\bar{l}^2\frac{(1-\upsilon)\lambda n^3}{2\lambda_c^3} + \bar{l}^2\frac{\overline{E_2}}{\overline{E_1}}\frac{(1-\upsilon)\lambda^3 n}{2\lambda_c} + \bar{l}^2\frac{\overline{E_2}}{\overline{E_1}}\frac{(1-\upsilon)\lambda n^3}{2\lambda_c^3},$$

$$\zeta_{13} = \zeta_{31} = \left(\upsilon_1 - \overline{Q_3}\right)\frac{-i\lambda}{\lambda_c} + \overline{Q_2}\frac{1}{\lambda_c^2} - \frac{\overline{E_2}}{\overline{E_1}}i\lambda^3 -$$
$$-\frac{\overline{E_2}}{\lambda_c^2\overline{E_1}}i\lambda^2\boldsymbol{n},$$

$$\zeta_{22} = -\left(\frac{1-\upsilon}{2} + \overline{Q_1} - (1+\upsilon)\alpha_1\overline{\Delta T}\right)\lambda^2 - 2\overline{Q_4}\frac{\lambda n}{\lambda_c} -$$
$$-\left(1+\overline{Q_3}\right)\frac{n^2}{\lambda_c^2} - \bar{l}^2\frac{1-\upsilon}{2}\lambda^4 - \bar{l}^2\frac{1-\upsilon}{2\lambda_c^2}\lambda^2 n^2 -$$
$$-\bar{l}^2\frac{\overline{E_2}}{\overline{E_1}}\frac{1-\upsilon}{2}\lambda^4 - \bar{l}^2\frac{\overline{E_2}}{\overline{E_1}}\frac{1-\upsilon}{2\lambda_c^2}\lambda^2 n^2 - \rho_s\frac{1-\upsilon^2}{\overline{E_1}}\bar{\omega}^2,$$

$$\zeta_{33} = \left(-\overline{Q_1} + (1+\upsilon)\alpha_1\overline{\Delta T}\right) - \lambda^2 + 2\overline{Q_4}\frac{\lambda n}{\lambda_c} - \overline{Q_3}\frac{n^2}{\lambda_c^2} + \frac{1}{\lambda_c^2} +$$
$$+\frac{h^2}{12\lambda_c^4} + \frac{\bar{h}^2}{12} + \frac{\overline{E_3}}{\overline{E_1}}\Delta\Delta - \frac{2\upsilon E_2}{\lambda_c E_1}\frac{\partial^2}{\partial x^2} + \frac{2\overline{E_2}}{\lambda_c^3\overline{E_1}}n^2 -$$
$$-\rho_s\frac{1-\upsilon^2}{\overline{E_1}}\bar{\omega}^2 + \bar{l}^2\frac{1-\upsilon}{2}\lambda^4 + \bar{l}^2\frac{1-\upsilon}{2\lambda_c^4}n^4 + \bar{l}^2\frac{1-\upsilon}{2\lambda_c^2}\lambda^2 n^2 +$$
$$+\bar{l}^2\frac{\overline{E_2}}{\overline{E_1}}\frac{1-\upsilon}{2}\lambda^4 + \bar{l}^2\frac{\overline{E_2}}{\overline{E_1}}\frac{1-\upsilon}{2\lambda_c^4}n^4 + \bar{l}^2\frac{\overline{E_2}}{\overline{E_1}}\frac{1-\upsilon}{2\lambda_c^2}\lambda^2 n^2.$$

Since the non-trivial solutions to Eq. (22) exist, we arrive at

$$|\zeta| = 0. \tag{26}$$

By expanding the determinant of Eq. (26), the characteristic polynomial is obtained in terms of dimensionless frequency.

From the characteristic polynomial, the dispersion relation curve of $\bar{\omega} - \bar{U}_o / \bar{V}_o$($\bar{V}_o / \bar{U}_o$ is given) will be obtained using the function 'ezplot' in the software package MATLAB. From the feature points of the given contour curve, we can determine the critical flow velocities associated with corresponding modes based on the judgment criterion of stability loss. The method is so-called 'the zero-level contour method'.

The judgment criterion of instability is given. When the backward wave crosses the zero-frequency line at point ($\overline{U_o}$=0.006012), the system loses its stability via divergence; When the forward and the backward travelling frequencies coalesce at 'nose' point C($\overline{U_o}$=0.09950), the

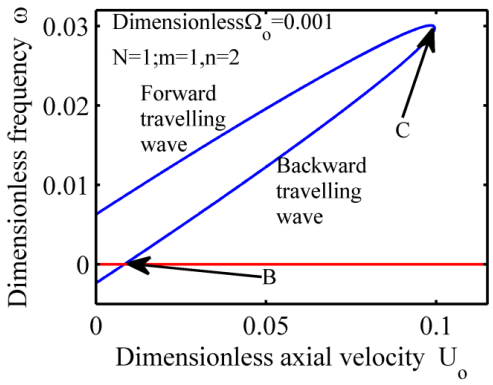

Fig. 2 Instability judgment criterion from the curve of frequency against axial flow velocity in the version of inviscid theory, $\Delta T = 0$

system loses its stability via coupled-mode flutter, as is shown in Fig. 2. With the increase in fluid rotation, the natural frequency of the system decreases dramatically. When the fluid rotation reaches a certain value, the divergence-type instability of the system disappears accordingly. Thus, the compound form of divergence and flutter becomes a single flutter.

3. Results and Discussion

3.1. Validation of the present method

There are few studies on the stability analysis of a micro-shell subjected to a swirling annular flow in the published literature. Therefore, an exact comparison between the present results and existing results is difficult to conduct. In order to evaluate the reasonableness and accuracy of the 'zero-level contour method', the annular flow is simplified to the internal flow with an axial velocity inside a micro-shell. The relevant geometric and material parameters for the micro-shell with simply- supported conditions are as follows [9]:

L = 100 μm, r = 10 μm, h = 0.1 μm, E = 1.44×10^{11} Pa, υ = 0.38, ρ_s = 1000kg m^{-3}, ρ_f = 1000kg m^{-3}, l = 17.6 μm.

It should be noted that the hydrodynamic pressure exerted on the inner wall of the shell by the internal fluid can be expressed as

$$p_i^i = -\rho_f \frac{L}{m\pi}\frac{I_n(\lambda)}{I_n'(\lambda)}\left(\frac{\partial}{\partial t}+U_o\frac{\partial}{\partial x}\right)w. \tag{27}$$

Thus, the entries ζ_{ij} in the matrix $\boldsymbol{\zeta}$ in Eq. (22) are accordingly rewritten as:

$$\zeta_{11} = -\lambda^2 - \frac{1-\upsilon}{2}n^2 - \bar{l}^2\frac{1-\upsilon}{4}\lambda^2 n^2 - \bar{l}^2\frac{1-\upsilon}{4}n^4 + \bar{\omega}^2,$$

$$\zeta_{12} = \zeta_{21} = \frac{1+\upsilon}{2}\lambda n + \bar{l}^2\frac{1-\upsilon}{4}\lambda^3 n + \bar{l}^2\frac{1-\upsilon}{4}\lambda n^3,$$

$$\zeta_{13} = \zeta_{31} = -i\upsilon\lambda,$$

$$\zeta_{22} = -\frac{1-\upsilon}{2}\lambda^2 - n^2 + \bar{\omega}^2 - \bar{l}^2\frac{1-\upsilon}{4}\lambda^4 - \frac{1-\upsilon}{4}\bar{l}^2\lambda^2 n^2,$$

$$\zeta_{22} = \zeta_{32} - \upsilon i n,$$

$$\zeta_{33} = 1 + \frac{\bar{h}^2}{12}\left(\lambda^2+n^2\right)^2 + \bar{l}^2\frac{1-\upsilon}{4^2}\lambda^4 + \bar{l}^2\frac{1-\upsilon}{4}n^4 +$$
$$+\bar{l}^2\frac{3(1-\upsilon)}{2}\lambda^2 n^2 - \bar{\omega}^2 - \frac{\bar{L}}{m\pi}\frac{\bar{I}_n(\lambda)}{\bar{I}_n'(\lambda)}\frac{1}{\bar{h}}\frac{\rho_f}{\rho_s}\left(\bar{\omega}-\lambda\bar{U}_o\right)^2.$$

The calculated dimensionless results with/without the size effect can be converted into dimensional results, listed in Table 1, and are compared with those reported in the literature [9].

Table 1
Comparisons of critical axial velocities for divergence instability of a simply supported micro-shell

	modified couple stress theory		classical continuum mechanics theory	
U_o, m/s	84.5571 [9]	85.7612 (present)	14.8067 [9]	13.9315 (present)
mode (m, n)	(1, 0)	(3, 1)	(1, 2)	(1, 1)

It can be seen from Table 1 that the present results agree well with those reported in the literature [9]. Furthermore, it can also be seen that the material length-scale parameter renders the critical axial velocities much higher than those predicted by the classical theory.

3.2. Dynamical stability analysis

In this study, we only consider the case of elastic outer and perfectly stiff inner shells. The size-dependent stability analysis of a micro-shell with/without temperature-dependent properties under an annular fluid are investigated. We adopt the simply supported boundary conditions to analyze the dynamical behavior of the micro-shell. The boundary conditions at the two edges $x = 0, L$ are expressed in terms of displacements

$$v_{i/o} = w_{i/o} = 0, \tag{28a}$$

$$r_{i/o}\frac{\partial u_{i/o}}{\partial x} + \upsilon\frac{\partial v_{i/o}}{\partial\theta} + \upsilon w_{i/o} - \frac{h_{i/o}^2}{12}\frac{\partial^2 w_{i/o}}{\partial x^2} = 0, \tag{28b}$$

Table 2
Two constituent material properties of S-FGMs micro-shell

Material	Properties	P_0	P_{-1}	P_1	P_2	P_3
Si_3N_4 (ceramic)	E, Pa	348.43e9	0	-3.70e-4	2.16e-7	-8.95e-11
	ρ, kg m^{-3}	2370	0	0	0	0
	α, K^{-1}	5.8723e-6	0	9.095e-4	0	0
SUS304 (steel)	E, Pa	201.04e9	0	0	-6.534e-7	0
	ρ, kg m^{-3}	8166	0	8.086e-4	0	0
	α, K^{-1}	12.33e-6	0	0	0	0
Water	ρ, kg m^{-3}	1000	0	0	0	0

$$r_{i/o}^2\frac{\partial^2 w_{i/o}}{\partial x^2}+\upsilon\frac{\partial^2 w_{i/o}}{\partial\theta^2}-\upsilon\frac{\partial v_{i/o}}{\partial\theta}-r_{i/o}\frac{\partial u_{i/o}}{\partial x}=0. \qquad (28c)$$

The material properties are listed in Table 2. For ease of comparison, we adopt the following geometric parameters: $L=$ 100 μm, $r=$ 10 μm, $k=(r_o-r_i)/r_i$, $r_i=9.0901$ μm, ($k=0$), $h=h_i=h_o=0.1$ μm, $l=h=0.1$, $\Delta/d=1.4865\times10^{-7}$.

Omitting the fluid viscous effects, we use the zero-level contour method to calculate the flow velocity associated with the different modes (m, n) by solving Eq. (26). From the obtained results, the lowest flow velocity of losing stability and the corresponding mode are found, as shown in Fig. 2. Also, in the case of considering the fluid viscous forces, similar results are obtained by the zero-level contour method based on the judgment criteria of stability loss.

3.2.1. Effects of material length-scale parameter

The material length-scale parameter l related to the size effect plays an important role in small-scale structures. For a micro-shell conveying fluid, the material length-scale parameter l can enhance the stability of such a system. The physical interpretation of the phenomenon is that the increase in strain energy induced by considering the size effect strengthens the ability of a micro-shell to resist buckling (static instability). In order to analyze the different stabilizing effects of couple forces $\bar{\gamma}_{ij}$ and couple moments $\bar{t}_{ij}$ related to the material length-scale parameter l quantitatively, the critical fluid velocities by divergence are calculated, as displayed in Figs. 3 and 4. From the two figures, the critical fluid velocities with couple forces $\bar{\gamma}_{ij}$ and couple moments $\bar{t}_{ij}$ are higher than those without them. Compared with the shear couple forces $\bar{\gamma}_{x\theta}$, $\bar{\gamma}_{xz}$, $\bar{\gamma}_{\theta z}$, the stabilizing effects of normal couple forces $\bar{\gamma}_x$, $\bar{\gamma}_\theta$ are obviously greater. However, the overall stabilizing effects of couple moments $\bar{t}_{ij}$ are insignificant.

The different stabilizing effects of the couple forces $\bar{\gamma}_{ij}$ and couple moments $\bar{t}_{ij}$ are summarized in Table 3. We find that the normal couple forces have the predominant stability effect while the stabilizing effect of shear couple forces is weak. The couple moments $\bar{t}_{ij}$ also have some stabilizing effects, though their overall contribution is minor. We can give the physical reason for the weak stabilizing effect of the couple moments $\bar{t}_{ij}$. For a micro-scale shell, the couple moments become very small in magnitude. Consequently, the couple moments $\bar{t}_{ij}$ offer a trivial stabilizing effect.

Table 3
Comparisons of dimensionless critical axial velocities for instability divergence in absence of $\bar{\gamma}_{ij}$ or $\bar{t}_{ij}$, $\bar{\Omega}_o=0.0001$, $\bar{U}_o=0.005035$

Absence of $\bar{\gamma}_{ij}$ or $\bar{t}_{ij}$	$\bar{U}'_o$	$\Delta\bar{U}_o=\bar{U}'_o-\bar{U}_o$	$\lvert\Delta\bar{U}_o\rvert/\bar{U}_o$
$\bar{\gamma}_x$, $\bar{\gamma}_\theta$	0.0042683	–0.00076740	15.24%
$\bar{\gamma}_{x\theta}$, $\bar{\gamma}_{xz}$, $\bar{\gamma}_{\theta z}$	0.0048211	–0.00021490	4.26%
$\bar{t}_x$, $\bar{t}_\theta$	0.0049280	–0.00010770	2.14%
$\bar{t}_{x\theta}$, $\bar{t}_{xz}$, $\bar{t}_{\theta z}$	0.0050265	–0.00000920	0.18%

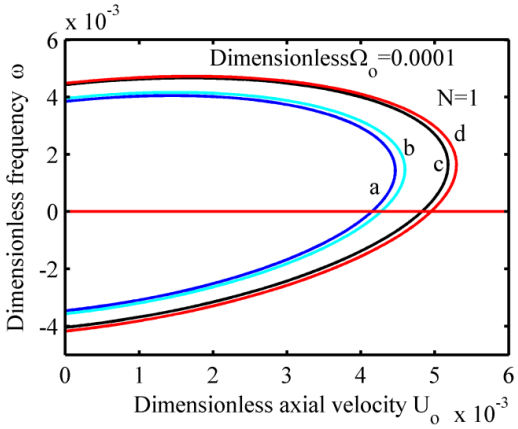

Fig. 3 Variation of frequency with axial flow velocity, $\Delta T=0$: a – without considering all couple forces and moments ($\bar{U}_o=0.004145$); b – without considering normal couple forces $\bar{\gamma}_x$, $\bar{\gamma}_\theta$ ($\bar{U}_o=0.004268$); c – without considering shear couple forces $\bar{\gamma}_{x\theta}$, $\bar{\gamma}_{xz}$, $\bar{\gamma}_{\theta z}$ ($\bar{U}_o=0.004821$); d – with considering all couple forces and moments ($\bar{U}_o=0.005035$)

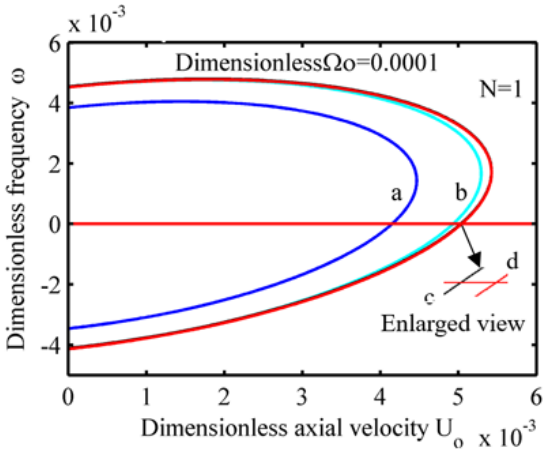

Fig. 4 Variation of frequency with axial flow velocity, $\Delta T=0$: a – without considering all couple forces and moments ($\bar{U}_o=0.004145$); b – without considering normal couple moments $\bar{t}_x$, $\bar{t}_\theta$ ($\bar{U}_o=0.004928$); c – without considering shear couple moments $\bar{t}_{x\theta}$, $\bar{t}_{xz}$, $\bar{t}_{\theta z}$ ($\bar{U}_o=0.005027$); d – with considering all couple forces and moments ($\bar{U}_o=0.005035$)

3.2.3. Effects of temperature

To verify the applicability and accuracy of the present formulation for the critical temperature rise, a traditional isotropic dry shell is considered with the following parameters:
$E=2.0\times10^{11}$ Pa, $\upsilon=0.3$, $\rho_s=8870$ kg m^{-3}, $L=1.5$ m, $r_o=0.2825$ m, $h_o=3.81\times10^{-4}$ m, $\alpha=12\times10^{-6}$ K^{-1}.

Fig. 5 shows a comparison between the present result and the published result [28], where the two temperature rise values ΔT by divergence are in reasonable agreement.

To facilitate physical understanding, the dimensionless temperature rise $\overline{\Delta T}$ was converted back to the dimensional temperature rise ΔT. Using the same geometric and material parameters in Subsection 3.2, Fig. 6 presents the effect of material property with or without dependent on

temperature on critical temperature rise ΔT by divergence of a dry S-FGMs micro-shell. It can be seen that the curve for temperature-independent material properties is higher than that for temperature-dependent ones. This is reasonable because the material properties are softened when the temperature dependence is considered.

To illustrate the influence of temperature rise ΔT on the stability behavior of an S-FGMs micro-shell, the stability boundaries under different temperature rises ΔT are shown in Fig. 7. We can see that the stability zones below and to the right of the curves shrink as the temperature rise ΔT increases. It indicates that the stability of the system diminishes with increasing temperature rise ΔT.

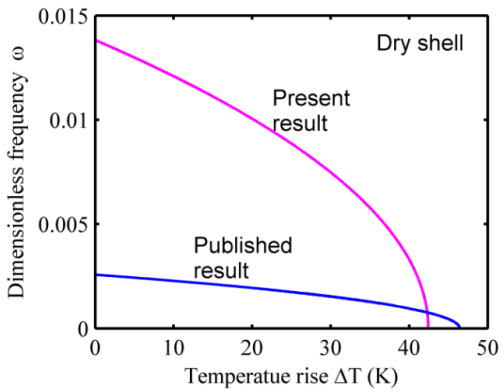

Fig. 5 Variation of frequency with temperature rise

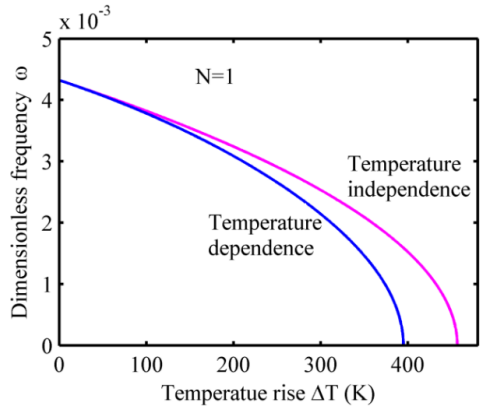

Fig. 6 Effects of temperature-dependent/temperature-independent material properties on critical temperature rise of a dry S-FGMs micro-shell

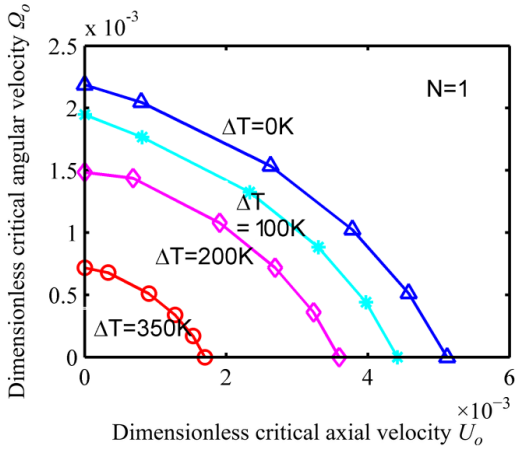

Fig. 7 Correlation curves of critical axial velocity versus critical angular velocity under different temperature rise

3.2.4. Effects of material parameter

Fig. 8 shows the influence of the volume ratio N on the stability behavior of such a system. From the figure, we can see that when N increases, three curves become lower, indicating weaker stability of the system. This is reasonable because the metal ratio increases with N, and a higher metal ratio usually corresponds to a lower elastic modulus.

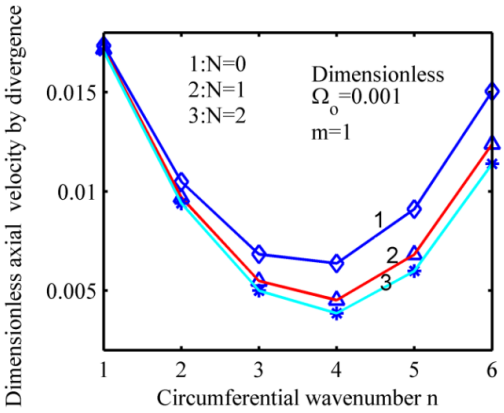

Fig. 8 Effects volume exponent N on critical axial velocities by divergence, ΔT = 100 K

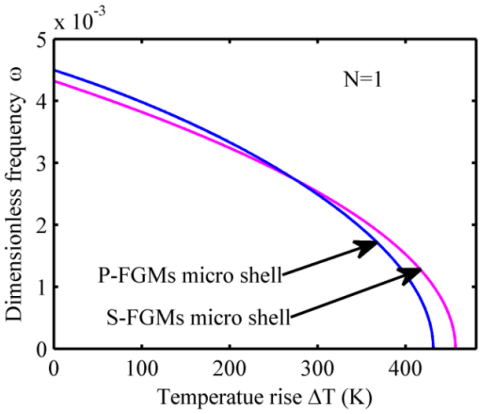

Fig. 9 Variation of dimensionless frequency with temperature rise by divergence for S-FGM and P-FGM micro-shells

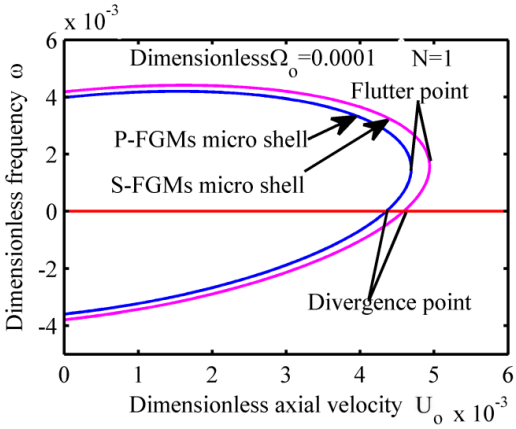

Fig. 10 Variation of dimensionless frequency with critical axial velocities by divergence for S-FGM and P-FGM micro-shells

Figs. 9 and 10 give a comparison between the present S-FGMs micro-shell and P-FGMs micro-shell. From the two figures, we can see that the critical temperature rise by divergence of the S-FGMs micro-shell is higher than that of the P-FGMs micro-shell. Furthermore, the critical fluid velocity by divergence of the S-FGMs micro-shell is also higher than that of P-FGMs micro-shell. In conclusion, the S-FGM micro-shell exhibits better stability than the P-FGM micro-shell. The material constituents can be modulated to control the stability of the system, which gives some insight into the design of micro-shell systems.

4. Concluding Remarks

To assess the effects of the couple forces/moments on the stability behaviors of an S-FGMs micro-shell under thermal loads, stability analyses were performed in the framework of modified couple stress theory and Love's shell theory. The inviscid hydrodynamic pressure and the viscous fluid forces are derived by using the inviscid and viscous theories. The shell motion equations are established using Hamilton's principle. Adopting the zero-level contour method, we obtain the travelling-wave type solutions for the simply supported outer shell motion equations. The obtained results, in good agreement with available data, demonstrate the feasibility of the proposed method.

The obtained results indicate that, the couple forces and couple moments related to the size effect do not qualitatively change the general stability of fluid-micro-shell system. However, all couple forces and couple moments do enhance the stability of the system. Moreover, the stabilizing effects are different. The normal couple forces exert the most remarkable stabilizing effect, while the stabilizing effect of the couple moments is much weaker.

The obtained results indicate that, the stability of the system decreases with increasing temperature rise. However, the temperature rise does not qualitatively affect the system instability mechanism. The stability of the S-FGMs micro-shell with temperature-dependent material properties is weaker than that with the temperature-independent material properties. In addition, the stability of the S-FGMs micro-shell with metal-ceramic-metal layers is better than that of the P-FGMs micro-shell with metal-ceramic layers.

Acknowledgements

The authors would like to gratefully acknowledge the support provided by the Huai'an natural science research plan projects (joint special projects) (No. HABL202206) and the Huai'an Key Research and Development Projects (No. HAG202205). The authors also thank the reviewers for their valuable suggestions.

References

1. **Bhushan, B.** 2007. Nanotribology and nanomechanics of MEMS/NEMS and BioMEMS/BioNEMS materials and devices, Microelectronic Engineering 84(3): 387-412. https://doi.org/10.1016/j.mee.2006.10.059.
2. **Yang, F.; Chong, A.C.M.; Lam, D.C.C.; Tong, P.** 2002. Couple stress based strain gradient theory for elasticity, International Journal of Solids and Structures 39(10): 2731-2743. https://doi.org/10.1016/S0020-7683(02)00152-X.
3. **Khorshidi, M.A.; Shariati, M.; Emam, S.A.** 2016. Postbuckling of functionally graded nanobeams based on modified couple stress theory under general beam theory, International Journal of Mechanical Sciences 110: 160-169. https://doi.org/10.1016/j.ijmecsci.2016.03.006.
4. **Lee, W.H.; Han, S.C.; Park, W.T.** 2015. A refined higher order shear and normal deformation theory for E-, P-, and S-FGM plates on Pasternak elastic foundation, Composite Structures 122: 330-342. https://doi.org/10.1016/j.compstruct.2014.11.047.
5. **Sahmani, S.; Ansari, R.; Gholami, R.; Darvizeh. A.** 2013. Dynamic stability analysis of functionally graded higher-order shear deformable microshells based on the modified couple stress elasticity theory, Composites Part B: Engineering 51: 44-53. https://doi.org/10.1016/j.compositesb.2013.02.037.
6. **Chung, Y.L.; Chi, S.H.** 2001. The residual stress of functionally graded materials, Journal of the Chinese Institute of Civil and Hydraulic Engineering 13(1): 1-9.
7. **Soleimani-Javid, Z.; Arshid, E.; Amir, S.; Bodaghi, M.** 2022. On the higher-order thermal vibrations of FG saturated porous cylindrical micro-shells integrated with nanocomposite skins in viscoelastic medium, Defence Technology 18(8): 1416-1434. https://doi.org/10.1016/j.dt.2021.07.007.
8. **Stone, H.A.; Kim, S.** 2001. Microfluidics: Basic issues, Applications, and Challenges, AIChE Journal 47(6): 1250-1254. https://doi.org/10.1002/aic.690470602.
9. **Zhou, X.; Wang, L.** 2012. Vibration and stability of micro-scale cylindrical shells conveying fluid based on modified couple stress theory, Micro and Nano Letters 7(7): 679-684. https://doi.org/10.1049/mnl.2012.0184.
10. **Mashrouteh, S.; Sadri, M.; Younesian, D.; Esmailzadeh, E.** 2016. Nonlinear vibration analysis of fluid- conveying microtubes, Nonlinear Dynamics 85: 1007-1021. https://doi.org/10.1007/s11071-016-2739-8.
11. **Hu, K.; Wang, Y.K.; Dai, H.L.; et al.** 2016. Nonlinear and chaotic vibrations of cantilevered micropipes conveying fluid based on modified couple stress theory, Int J Eng Sci 105: 93–107. https://doi.org/10.1016/j.ijengsci.2016.04.014.
12. **Jannesari, H.; Emami, M.D.; Karimpour, H.** 2012. Investigating the effect of viscosity and nonlocal effects on the stability of SWCNT conveying flowing fluid using nonlinear shell model, Physics Letters A 376(12-13): 1137–1145. https://doi.org/10.1016/j.physleta.2012.02.008.
13. **Arani, A.G.; Haghparast, E.; Rarani, M.H.; Maraghi, Z.K.** 2015. Strain gradient shell model for nonlinear vibration analysis of visco-elastically coupled Boron Nitride nano-tube reinforced composite micro-tubes conveying viscous fluid, Computational Materials Science 96: 448-458. https://doi.org/10.1016/j.commatsci.2014.06.013.
14. **Babaei, H.; Eslami, M.R.** 2022. Nonlinear bending analysis of size-dependent FG porous microtubes in thermal environment based on modified couple stress

theory, Mechanics Based Design of Structures and Machines 50(8): 2714-2735. https://doi.org/10.1080/15397734.2020.1784202.
15. **Wang, L.; Ni, Q.; Li, M.; Qian, Q.** 2008. The thermal effect on vibration and instability of carbon nanotubes conveying fluid, Physica E: Low-dimensional Systems and Nanostructures 40(10): 3179-3182. https://doi.org/10.1016/j.physe.2008.05.009.
16. **Askari, H.; Esmailzadeh, E.** 2017. Forced vibration of fluid conveying carbon nanotubes considering thermal effect and nonlinear foundations, Composites Part B: Engineering 113: 31-43. https://doi.org/10.1016/j.compositesb.2016.12.046.
17. **Ghavanloo, E.; Fazelzadeh, S.A.** 2011. Flow-thermoelastic vibration and instability analysis of viscoelastic carbon nanotubes embedded in viscous fluid, Physica E: Low-dimensional Systems and Nanostructures 44(1): 17-24. https://doi.org/10.1016/j.physe.2011.06.024.
18. **Tong, G.J.; Liu, Y.S.; Liu, H.C.; Dai, J.Y.** 2019. Thermoelastic vibration analysis of micro-scale functionally graded material fluid-conveying pipes in elastic medium, Journal of Central South University 26: 2785-2796. https://doi.org/10.1007/s11771-019-4213-5.
19. **Ning, W.B.; Li, Y.D.; Chen, Z.; Chen, X.G.; Wang, S.Y.** 2022. Influence of swirl and viscosity of annular flow on instability mechanisms of an FGMs micro shell, Applied Mathematical Modelling 104: 386-400. https://doi.org/10.1016/j.apm.2021.12.014.
20. **Layeghi, M.; Seyf, H.R.** 2008. Fluid Flow in an Annular Microchannel Subjected to Uniform Wall Injections, ASME Journal of Fluids Engineering 130(5): 054502. https://doi.org/10.1115/1.2911655.
21. **Pfund, D.; Rector, D.; Shekarriz, A.; Popescu, A.; Welty, J.** 2000. Pressure drop measurements in a microchannel, AIChE Journal 46(8): 1496-1507. https://doi.org/10.1002/aic.690460803.
22. **Haaland, S.E.** 1983. Simple and Explicit Formulas for the Friction Factor in Turbulent Pipe Flow, ASME Journal of Fluids Engineering 105(1): 89-90. https://doi.org/10.1115/1.3240948.
23. **Brighton, J.A.; Jones, J.B.** 1964. Fully Developed Turbulent Flow in Annuli, ASME J. Basic Eng. 86(4): 835-842. https://doi.org/10.1115/1.3655966.
24. **Touloukian, Y.S.** 1967. Thermophysical Properties of High Temperature Solid Materials: Elements (Vol. 1), New York: Macmillan.
25. **Love, A.E.H.** 1952. A Treatise on the Mathematical Theory of Elasticity, 4th Ed. Cambridge: Cambridge University Press.
26. **Eslami, M.R.; Ziaii, A.R.; Ghorbanpour, A.** 1996. Thermoelastic buckling of thin cylindrical shells based on improved stability equations, Journal of Thermal Stresses 19(4): 299-315. https://doi.org/10.1080/01495739608946177.
27. **Zhang, X.M.; Liu, G.R.; Lam, K.M.** 2001. Coupled vibration analysis of fluid-filled cylindrical shells using the wave propagation approach, Applied Acoustics 62(3): 229-243. https://doi.org/10.1016/S0003-682X(00)00045-1.
28. **Ning, W.B.; Hu, G.Z.; Chen, G.Y.** 2016. Dynamic stability analysis of a cylindrical shell subjected to swirling annular flow under thermal loads, International Journal of Mechanical Sciences 115-116: 689-701. https://doi.org/10.1016/j.ijmecsci.2016.07.043.

W.B. Ning, X. Xu, Y. Zhou

DYNAMIC STABILITY OF AN S-FGMS MICRO SHELL WITH TEMPERATURE–DEPENDENT PROPERTIES SUBJECTED TO A SWIRLING ANNULAR FLOW CONSIDERING FLUID VISCOSITY

S u m m a r y

The theoretical model was developed for predicting the stability behavior of a micro-shell subjected to swirling fluid in the annular gap between the inner shell and outer shell, where the shell material properties are characterized by sigmoid functionally graded materials (S-FGMs) and are dependent on temperature. The theoretical formulation was based on the modified couple stress theory and Love's shell theory. The fluid forces include two parts: the inviscid fluid hydrodynamic pressure and the steady viscous forces. Hamilton's principle was used to derive the governing motion equations of a shell under fluid forces and thermal loads. The zero-level contour method and the travelling-wave approach were utilized to reveal the complex dynamical behaviors of micro-shell. The different stabilizing effects of couple forces and moments induced by the size effect are discussed fully. It could be found that the thermal loads markedly reduce the shell stability and the stability is markedly affected when considering shell material properties dependent on temperature. Furthermore, the effect of shell material parameter on the stability behavior of the fluid-micro-shell system was studied.

Keywords: micro shell, couple force, thermal loads.

Received March 8, 2026
Accepted October 15, 2026

This article is an Open Access article distributed under the terms and conditions of the Creative Commons Attribution 4.0 (CC BY 4.0) License (http://creativecommons.org/licenses/by/4.0/).